metals

MDPI

Article

First-Principles Study of Structural Stability and Mechanical Properties of Ta–W–Hf Alloys

Xudong Ran, Shuhai Huang, Shaolan Zhou, Wei Lei, Yang Wu and Qiang Chen *

Southwest Technology and Engineering Research Institute, Chongqing 400039, China; xudongran0828@outlook.com (X.R.)
* Correspondence: 2009chenqiang@163.com; Tel.: +86-023-68792167

Abstract: In order to obtain the effect of W and Hf elements on the mechanical properties of Ta–W–Hf alloys, the structural, mechanical, and electronic properties of Ta–xW–6.25Hf (x = 6.25, 12.50, 18.75, 25.00, 31.25, 50.00) alloys were studied using first-principles calculation based on density functional theory, and the supercell method. The calculated formation enthalpy and elastic constants clarify that Ta–W–Hf alloys have structural and dynamical stability. The formation enthalpy and the cohesive energy decrease with the increase in W content, and the cohesive energy increases when Hf element is added to Ta–W alloy. In addition, bulk modulus (B), shear modulus (G), and Young's modulus (E) for each of the Ta–xW alloys increase gradually with the increase in W concentration. The B, G, and E of Ta–xW–6.25Hf alloys is lower than that of Ta–xW alloy under the same W content conditions, suggesting that Hf alloying with higher Ta–W concentration becomes softer than the Ta–W alloy. Based on the mechanical characteristic, the B/G and Poisson's ratio of Ta–W–Hf alloys are higher than those of Ta–W alloys with W content over 25%, the ductility of Ta–W–Hf alloys improves with the addition of Hf, and Hf can reduce the anisotropy of Ta–W–Hf alloys. Furthermore, the electronic density of states shows that alloying W and Hf improves the metallicity of Ta. The results in this work provide the underlying insights needed to guide the design of Ta–W–Hf alloys with excellent mechanical properties.

Keywords: first-principles calculation; Ta–W–Hf alloys; structural stability; elastic properties

Citation: Ran, X.; Huang, S.; Zhou, S.; Lei, W.; Wu, Y.; Chen, Q. First-Principles Study of Structural Stability and Mechanical Properties of Ta–W–Hf Alloys. *Metals* **2023**, *13*, 655. https://doi.org/10.3390/met13040655

Academic Editor: Diego Celentano

Received: 13 February 2023
Revised: 17 March 2023
Accepted: 23 March 2023
Published: 25 March 2023

1. Introduction

With its high melting point, high density, excellent ductility, and high strength, tantalum (Ta) has been considered a key material for future nuclear fusion reactors [1–3]. Tungsten (W) has physical properties similar to tantalum and can be solidly soluble in Ta indefinitely. Due to solid-solution strengthening, Ta–W alloys are stronger than pure Ta and are widely used in the nuclear engineering, weaponry, and aerospace industries [4–6]. For example, Ta–2.5W can be used in heat exchangers; Ta–7.5W is a spring material for corrosion-resistant equipment; and Ta–10W is a key material of choice for liquid rocket engine thrust combustion chambers, vacuum furnace heaters, and other high-temperature components. Ta–W alloys are widely studied because of their excellent application potential. Li [7] studied the valence bond structure of a body-centered cubic (BCC) Ta–W alloy based on characteristic crystal (CC) theory and analyzed the mechanism of solid-solution strengthening of Ta–W alloys. Lv et al. [8] studied the stability of alloying elements W and its interaction with vacancy defects in Ta–W alloys based on the first-principles study. The results show that W atoms are more likely to disperse in the Ta lattice, and are less likely to form precipitates even with vacancy coexistence, thus, W can be doped into Ta-based materials as a point defect repair element. Wang et al. [9] reported that the increase in W content resulted in the enhancement of α-fibers and weakening of γ-fibers in Ta–W alloys. For example, the volume fraction of γ-fibers in Ta–10W alloy is lower than that of Ta–2.5W alloy. Zhang et al. [10] prepared Ta–W refractory alloys with W contents ranging from 10%

to 50% (atomic content) by arc melting, and the results showed that the compressive yield strength of Ta–W alloys increased with W concentration at both temperatures, and they exhibited excellent high-temperature compressive strength. In particular, the strength of the Ta–20%W alloy reached as high as 236 MPa at 2000 °C. Ma's work showed that Ta–W alloys are good construction materials for equipment handling aggressive acidic media, and that cold-rolled Ta–4%W plates combine strength and corrosion resistance [11].

Based on the study of Ta–W alloys, the researchers found that the addition of Hf elements can improve the corrosion resistance and creep resistance of Ta–W alloys. As a backflow snake tube, the Ta–10W alloy experienced severe potassium corrosion at 980 °C, while the Ta–8%W–2%Hf alloy did not experience corrosion at 1315 °C for 2000 h [12,13]. Zhang et al. [14,15] prepared Ta–W–Hf alloys and analyzed their strengthening and grain boundary hardening processes, and the results show that the Ta–W–Hf material deforms with good continuity, does not produce strong local deformation, and exhibits plastic fracture. Leonard et al. [16] studied the tissue changes and factors affecting the mechanical properties of the Ta–2%W–2%Hf (T111) alloy with thermal aging times of 1100 h at 1098 K, 1248 K, and 1398 K. It was shown that the resistivity and strength of the material decreased with increasing aging temperature, and the same pattern was obtained by Distefano [17] when studying the mechanical properties of a Ta–8W–2Hf alloy at 300–650 °C. Senkov et al. [18] studied the mechanical properties of a Hf–27%Ta alloy and a Hf–21%Ta–21%W alloy at different temperatures, and the result show both alloys still have good processing properties when the temperature exceeds 1000 °C. In addition, the researcher [19] studied the organization, mechanical properties, and oxidation behavior of a Hf–25%Ta–5%W (HTW) alloy below the co-precipitation temperature. The experiment showed that the yield stress of the HTW alloy was strongest at 25 °C (σ_y = 1966 MPa) and the room temperature plasticity of the alloy increased with the decrease in σ_y. The HTW alloy maintained high strength at 800 °C. By comparing the oxidation behavior of the Hf–25Ta binary alloy at 800 °C and 1000 °C, the oxidation resistance of the alloy is improved with the addition of Hf. Barklay et al. [20] analyzed the microstructural properties of Ta–10%W and Ta–8%W–2%Hf alloys, which shows that Ta–8%W–2%Hf has better internal damage accumulation and resistance to radiation than Ta–10%W [21].

In summary, researchers have conducted a large number of studies on Ta–W and Ta–W–Hf alloys, but, up to now, there still have not been systematic studies to investigate the mechanical properties of Ta–W–Hf alloys from the atomic scale. The basic property parameters of the Ta–W–Hf alloys remain to be supplemented. Ta is a refractory alloy, which requires huge costs to prepare by traditional methods, and there is a certain degree of danger, which cannot meet a variety of needs for alloy development. With the development of computer science, computer simulation technology has become an important tool for material design and analysis. Alloy composition screening, and processing process optimization can be performed quickly by computer, which will reduce the workload and shorten the development cycle. In addition, it has a guiding role in clarifying the reaction mechanism and the development of the alloy.

In this work, we established 12 atoms models by supercell method, and calculated the formation energy and cohesion energy of Ta–W and Ta–W–6.25Hf alloys with different W content, based on the first-principles method. Next, we calculated the elastic constants of these alloys. Finally, according to the Voigt–Reuss–Hill approximation, we obtained property parameters such as Young's modulus, bulk modulus, and shear modulus, as well as Poisson's ratio. The results of these calculations will be quite helpful for understanding the basic physical properties of Ta–W–Hf alloys, which provide theoretical predictions for optimizing the properties of Ta–W–Hf alloys.

2. Methods and Details

2.1. Calculation Methods

A method based on the density functional theory was performed in the CASTEP module of the Materials Studio [22]. The ultra-soft pseudo-potential plane-wave is used

to modified the core ions and valence electrons interaction, and the exchange–correlation part is described with the generalized gradient approximation (GGA) by Perdew–Burke–Ernzerhof (PBE). Through the convergence test, the plane wave cutoff energy was selected as 400 eV, and the Monkhorst–Pack k-points were selected to be 18 × 18 × 18. Before the calculation, the Broyden–Fletcher–Goldfarb–Shanno (BFGS) method was used to optimize the structure of the cell. After obtaining the local most stable structure, the next step was calculated. The Pulay density mixing method was used to accelerate the self-consistent cycle. In the geometry optimization progress the convergence precision of iteration is 10^{-5} eV/atom.

The components of the elastic tensor C_{ij} were calculated by computing the stress–strain relationships. According to the continuous elastic theory, the cubic crystal system has three independent elastic constants. The elastic constants are C_{11}, $C_{12,}$ and C_{44}, which represent three equal elastic constants ($C_{11} = C_{22} = C_{33}$; $C_{12} = C_{23} = C_{31}$; $C_{44} = C_{55} = C_{66}$). The matrix of elastic constants for cubic crystals is given below:

$$[C] = \begin{bmatrix} C_{11} & C_{12} & C_{12} & 0 & 0 & 0 \\ C_{12} & C_{11} & C_{12} & 0 & 0 & 0 \\ C_{12} & C_{12} & C_{11} & 0 & 0 & 0 \\ 0 & 0 & 0 & C_{44} & 0 & 0 \\ 0 & 0 & 0 & 0 & C_{44} & 0 \\ 0 & 0 & 0 & 0 & 0 & C_{44} \end{bmatrix} \quad (1)$$

C_{11} describes the resistance of the material to a change in its length caused by an axial stress applied in the (100) plane in the <100> direction. C_{12} indicates the resistance of the material to deformation as a result of axial (longitudinal) stresses in the (100) plane in the <010> direction. C_{44} is the resistance of the material to deformation owing to the application of tangential shear stress in the (010) plane in the <001> direction.

To obtain the elastic constants C_{11}, $C_{12,}$ and C_{44}, three specific strains (δ) are applied in different directions to the cubic supercell. A quadratic functional relationship between the total energy change (ΔE) and the strain (δ) is constructed based on Hooks' law. This relationship is given in Table 1.

Table 1. Relationships between strain (δ) and total energy change (ΔE) for a cubic crystal system.

Strain	Change of Total Energy
e = (0,0,0, δ, δ, δ)	$\frac{\Delta E}{V} = \frac{3}{2} C_{44} \delta^2$
e = (δ, δ,0, 0, 0, 0)	$\frac{\Delta E}{V} = (C_{11} + C_{12}) \delta^2$
e = (δ, δ, δ, 0, 0, 0)	$\frac{\Delta E}{V} = \frac{3}{2} (C_{11} + 2C_{12}) \delta^2$

2.2. Calculation Models

In this calculation, all models are established by 2 × 2 × 2 supercell in a body-centered cubic structure (bcc), and replacing Ta atoms at positions with W/Hf atoms. Since the atomic radius ratio of W/Hf to Ta is much larger than 0.59, the possibility of forming interstitial solid solution is small, so this work mainly considers W/Hf in Ta as a replacement. Ta atoms are substituted by W and/or Hf atoms to obtain various alloys. These are: Ta–6.25W, Ta–12.5W, Ta–18.75W, Ta–25.00W, Ta–31.25W, Ta–50.00W, Ta–6.25W–6.25Hf, Ta–12.5W–6.25Hf, Ta–18.75W–6.25Hf, Ta–25.00W–6.25Hf, Ta–31.25W–6.25Hf, and Ta–50.00W–6.25Hf, where the numbers refer to the atomic percentages (at%) of the alloys, the same as in the following. All of structures are shown in Figures 1 and 2. The purple, red, and green atoms are Ta, W, and Hf, respectively.

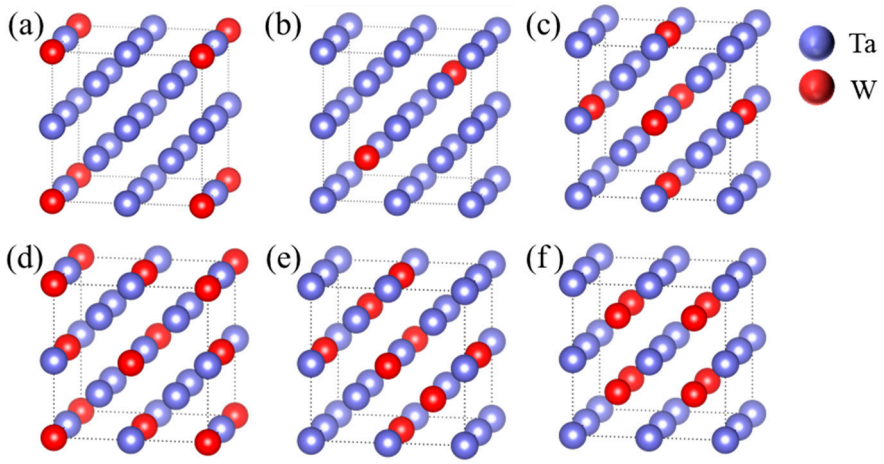

Figure 1. Atomic structure models of Ta–W alloys. (**a**) Ta–6.25W, (**b**) Ta–12.5W, (**c**) Ta–18.75W, (**d**) Ta–25.00W, (**e**) Ta–31.25W, (**f**) Ta–50.00W.

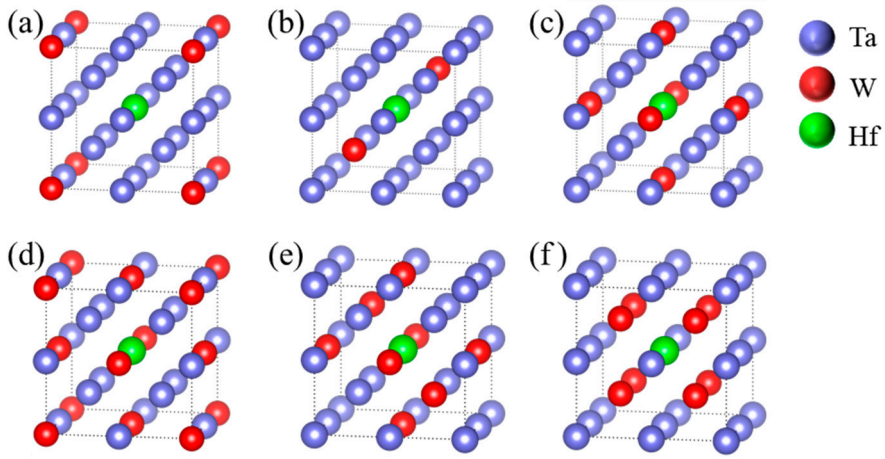

Figure 2. Atomic structure models of Ta–W–Hf alloys. (**a**) Ta–6.25W–6.25Hf, (**b**) Ta–12.5W–6.25Hf, (**c**) Ta–18.75W–6.25Hf, (**d**) Ta–25.00W–6.25Hf, (**e**) Ta–31.25W–6.25Hf, (**f**) Ta–50.00W–6.25Hf.

3. Results and Discussion

3.1. Calculation Model and Method Verification

In order to verify the accuracy of the calculations, the choice of supercell sizes and the calculation results are compared with the available experimental results in this work. All possible choices of supercell sizes have been considered in the preliminary stages of model construction. The results show that the calculations for the models under consideration are all in agreement with the experimental results, so, considering the reasonable utilization of computing resources, a $2 \times 2 \times 2$ supercell was used for the calculations.

In addition, the results for the Ta–W–Hf alloys were validated and compared with previous studies in this work. However, ternary Ta–W–Hf alloys have never been reported. In this work, the lattice constant and elastic modulus of Ta–W alloys is reported in Sections 3.2 and 3.3, respectively. As shown, the lattice constant decreases and the elastic modulus increases with increasing W content, and these results are consistent with the results of previous studies [10,23]. This suggests that the results of the calculations in this study are reasonable.

3.2. Crystal Structure Parameters and Structural Ability

3.2.1. Lattice Constants

Firstly, we optimized the structure of the selected cells of the Ta–W–Hf alloys; the results of the optimized lattice constants are listed in Table 2. Figure 3 shows the relationships

between the lattice constants and W content of Ta–W–Hf alloys. As shown in Figure 3, the calculated values in this work are in good agreement with the experiment data and the results obtained by other calculation methods, with the average deviations being less than 1.2%, which confirms that the models and calculational parameters are reliable. The following works are carried out on this basis.

Table 2. Atom fraction and lattice constant of different density components of Ta–W–Hf alloys.

Alloys	W (at. %)	Hf (at. %)	W (wt. %)	Ta (wt. %)	a/Å	Note
Ta	0.000	0.000	0.000	-	3.363	Present
Ta	-	-	-	-	3.312	Cal [23]
Ta	-	-	-	-	3.306	Exp [24]
Ta–6.25W	6.250	0.000	6.410	0.000	3.349	Present
Ta–12.50W	12.50	0.000	12.680	0.000	3.335	Present
Ta–18.75W	18.75	0.000	21.100	0.000	3.321	Present
Ta–25.00W	25.00	0.000	25.300	0.000	3.308	Present
Ta–31.25W	31.25	0.000	31.590	0.000	3.296	Present
Ta–50.00W	50.00	0.000	50.400	0.000	3.251	Present
Ta–50.00W	-	0.000	-	0.000	3.263	Cal [23]
Ta–6.25W–6.25Hf	6.250	6.250	6.410	-	3.362	Present
Ta–12.5W–6.25Hf	12.50	6.250	12.680	-	3.347	Present
Ta–18.75W–6.25Hf	18.75	6.250	21.100	-	3.332	Present
Ta–25.00W–6.25Hf	25.00	6.250	25.300	-	3.319	Present
Ta–31.25W–6.25Hf	31.25	6.250	31.620	-	3.303	Present
Ta–50.00W–6.25Hf	50.00	6.250	50.400	-	3.269	Present

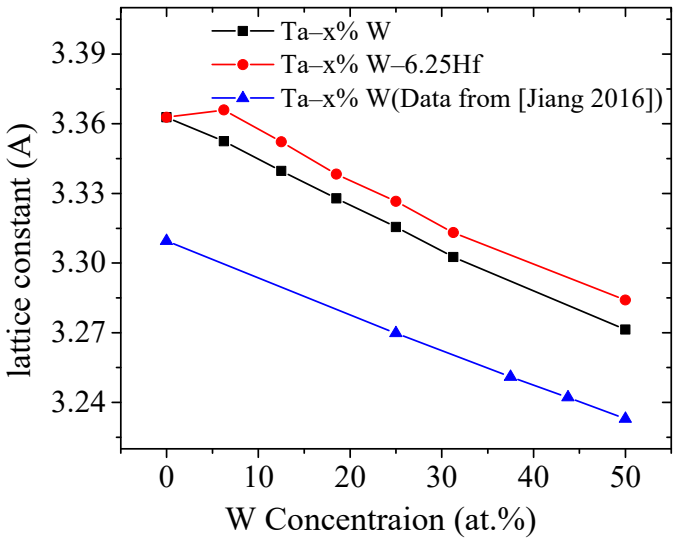

Figure 3. Relationships between the lattice constant and W content of Ta–W alloys. Data from Jiang [23].

From Figure 3, it can be seen that the lattice constant of the Ta–W alloy decreases linearly with increasing W content, while it increases when Hf is added to Ta–W, which is mainly due to the atomic radius of W > Ta > Hf. The variation in the lattice constant satisfies Vegard's law, and the relationship between the lattice constant and W content is obtained as given below:

$$a = \left(3.230 \pm 6.561E^{-4}\right) + \left(-0.0036 \pm 5.560E^{-5}\right)x \quad (2)$$

where x refers to the numbers of W.

3.2.2. Formation Energy and Cohesive Energy

The stability of the alloy has great influence on the mechanical properties of the material. In order to study the stability of W element in Ta–W–Hf alloys, the formation energy

and cohesive energy of Ta–W alloys under different doping W contents are calculated. The formation energy and cohesive energy are calculated according to the following equations:

$$E_f = \frac{-E_{tot}^{TaW} + ME_{bulk}^{Ta} + NE_{bulk}^{W}}{M+N} \quad (3)$$

$$Ecoh = \frac{-E_{tot}^{TaW} + ME_{single}^{Ta} + NE_{single}^{W}}{M+N} \quad (4)$$

where E_{tot}^{TaW} is the total energy of the Ta–W system, E_{bulk}^{Ta}, E_{bulk}^{W} are the total energy of *Ta* and *W* in the solid state of ground state, respectively. E_{single}^{Ta}, E_{single}^{W} are the total energy of *Ta* and *W* atoms in isolation state, respectively; *M* and *N* are the number of *Ta* and *W* atoms, respectively.

The formation energy and cohesive energy of Ta–W alloys and Ta–W–Hf alloys with different doping W contents calculated by the equation are shown in Figure 4 below. The cohesive energy represents the energy difference between the crystal state and the free atomic state of the atoms forming the crystal. A negative value of the cohesive energy indicates that the crystal is stable, and a more negative value indicates a more stable crystal structure. As shown in Figure 4a,b, when the Ta alloy is doped with W and Hf elements, the formation energy and cohesive energy are negative, indicating that the Ta–W–Hf alloy can form spontaneously and exist stably when the W content is lower than 50%. The absolute value of cohesive energy increases with the increase in W content, indicating that the stability of the Ta–W alloy increases with the increase in W content, while the absolute value of cohesive energy decreases when Hf element is added to the Ta–W alloy, indicating that Hf can reduce the stability of the Ta–W alloy.

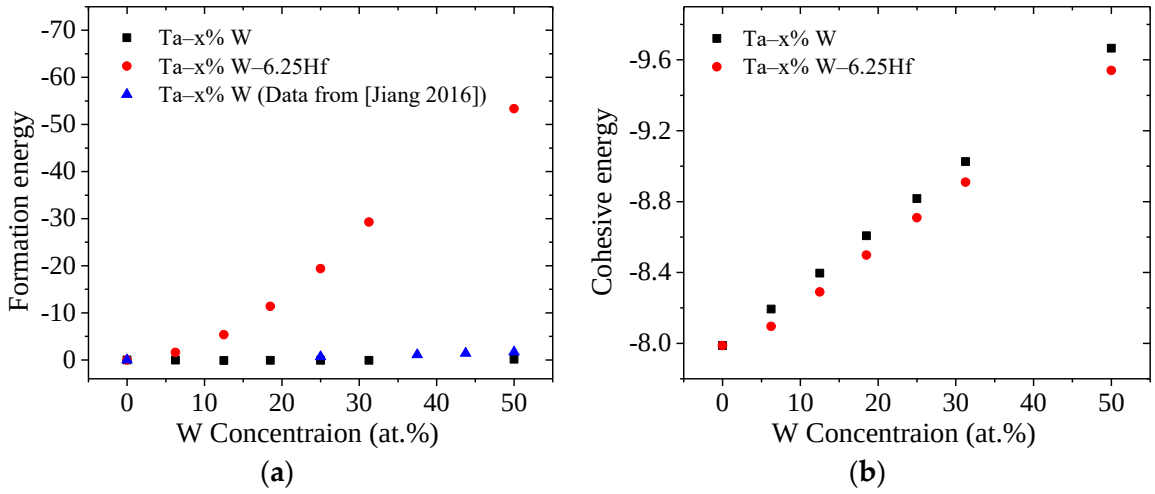

Figure 4. The formation energy and cohesive energy of Ta–W alloy and Ta–W–Hf alloy with different doping W contents: (**a**) the formation energy, (**b**) the cohesive energy. Data from Jiang [23].

3.3. Mechanical Properties

The mechanical properties are important parameters for the design and characterization of alloys, where the elastic properties, as one of the important mechanical properties of the material, describe the occurrence of deformation of the material under the action of external forces. The main constants indicating the elastic properties of the material are the bulk modulus, shear modulus, and other physical quantities, which can be obtained in Castep [25,26].

The cubic structure has three independent elastic parameters, namely, C_{11}, C_{12}, and C_{44}. According to the Voigt–Reuss–Hill scheme [27,28], other elastic parameters, such as bulk modulus (B), Young's modulus (E), shear modulus (G), Poisson's ratio (σ) and

anisotropy coefficients (A), etc., can be gained by taking the elastic constants C_{11}, $C_{12,}$ and C_{44} as shown below:

$$B_v = B_R = \frac{1}{3}(C_{11} + 2C_{12}) \tag{5}$$

$$C_v = \frac{1}{5}(C_{11} - C_{12} + 3C_{44}) \tag{6}$$

$$C_R = \frac{5C_{44}(C_{11} - C_{12})}{4C_{44} + 3(C_{11} - C_{12})} \tag{7}$$

$$E = \frac{9BG}{3B + G} \tag{8}$$

$$\sigma = \frac{3B - 2G_H}{2(3B + 2G_H)} \tag{9}$$

$$A = \frac{2C_{44}}{C_{11} - C_{12}} \tag{10}$$

where v, R, and H indicate Voigt, Reuss, and Hill, respectively. According to the 'Born stability criteria', we can understand the mechanical stability of cubic crystals [29,30]. The 'Born stability criteria' are as follow: $C_{11} > 0$, $C_{44} > 0$, $C_{11} - C_{12} > 0$.

3.3.1. Elastic Properties

Table 3 shows the calculated elastic constants and modulus of Ta–W alloys and Ta–W–Hf alloys with different W contents. All of the Ta–W alloys are mechanically stable because they all satisfy the Born stability criteria. As shown in Figure 5, when W is added to the Ta–W alloy, the elastic constants C_{11}, C_{12}, and C_{44} increase with the increase in the W concentration. When Hf is added to the Ta–W–Hf alloy, the change trend of the elastic constants C_{11} and C_{12} is consistent with that of the Ta–W alloy, while the increase amplitude is lower than that of the Ta–W alloy. For Ta–W–Hf alloys, C_{44} firstly increases and then decreases with the increase in W content. When W content reaches 50%, the minimum value of C_{44} reaches 46.33 GPa.

The modulus of elasticity is an important mechanical index used to describe the elasticity of a substance and reflects the macroscopic properties of the material. Table 4 shows the calculated constants of bulk modulus (B), shear modulus (G), and Young's modulus (E) with W content for Ta–W alloys and Ta–W–Hf alloys. As can be seen, under the same condition of doping W content, all the physical quantities of B, G, and E of the Ta–W alloys are larger than those of Ta–W–Hf, which means the mechanical strengths are somewhat reduced with the addition of Hf elements in Ta–W–Hf alloys. In the Ta–W alloy, all three elastic moduli increase with increasing W content. However, when Hf solid solution is added into Ta–W, the bulk modulus of the Ta–W–Hf alloy increases with the increase in W content. The bulk modulus increases from 318.43 GPa of Ta–50W–6.25Hf to 252.11 GPa of Ta–6.25W–6.25Hf, and increases by 21.4% compared with the pure Ta alloy. Bulk modulus is used to characterize the ability of the material volume to resist external forces. With the increase in W content, the bulk modulus of the Ta–W–Hf alloy increases, and its compression resistance is enhanced.

Table 3. The calculated elastic constant of Ta–W alloys with different W content (unit: GPa).

Alloy	C_{11}	C_{12}	C_{44}	C_{12}–C_{44}	Note
Ta	261.74	160.37	51.39	108.98	Present
Ta	262.38	159.05	56.99	102.06	Cal [31]
Ta	277.87	167.37	62.87	104.50	Cal [23]
Ta	245.18	159.8	67.58	92.22	Exp [32]
Ta–6.25W	266.25	153.73	51.60	102.13	Present
Ta–12.50W	285.52	170.24	53.96	116.28	Present
Ta–18.75W	289.00	172.61	52.96	119.65	Present
Ta–25.00W	295.10	173.60	53.22	120.38	Present
Ta–25.00W	320.60	180.10	60.01	120.09	Cal [23]
Ta–31.25W	311.85	179.92	55.67	124.26	Present
Ta–50.00W	358.34	186.80	55.93	130.87	Present
Ta–50.00W	375.72	195.85	75.48	120.37	Cal [23]
Ta–6.25W–6.25Hf	252.11	156.65	47.19	204.92	Present
Ta–12.5W–6.25Hf	270.38	159.33	53.08	217.30	Present
Ta–18.75W–6.25Hf	281.87	164.94	54.70	227.17	Present
Ta–25.00W–6.25Hf	288.54	170.16	53.21	235.33	Present
Ta–31.25W–6.25Hf	307.87	182.41	52.31	255.55	Present
Ta–50.00W–6.25Hf	318.43	193.84	46.33	272.11	Present

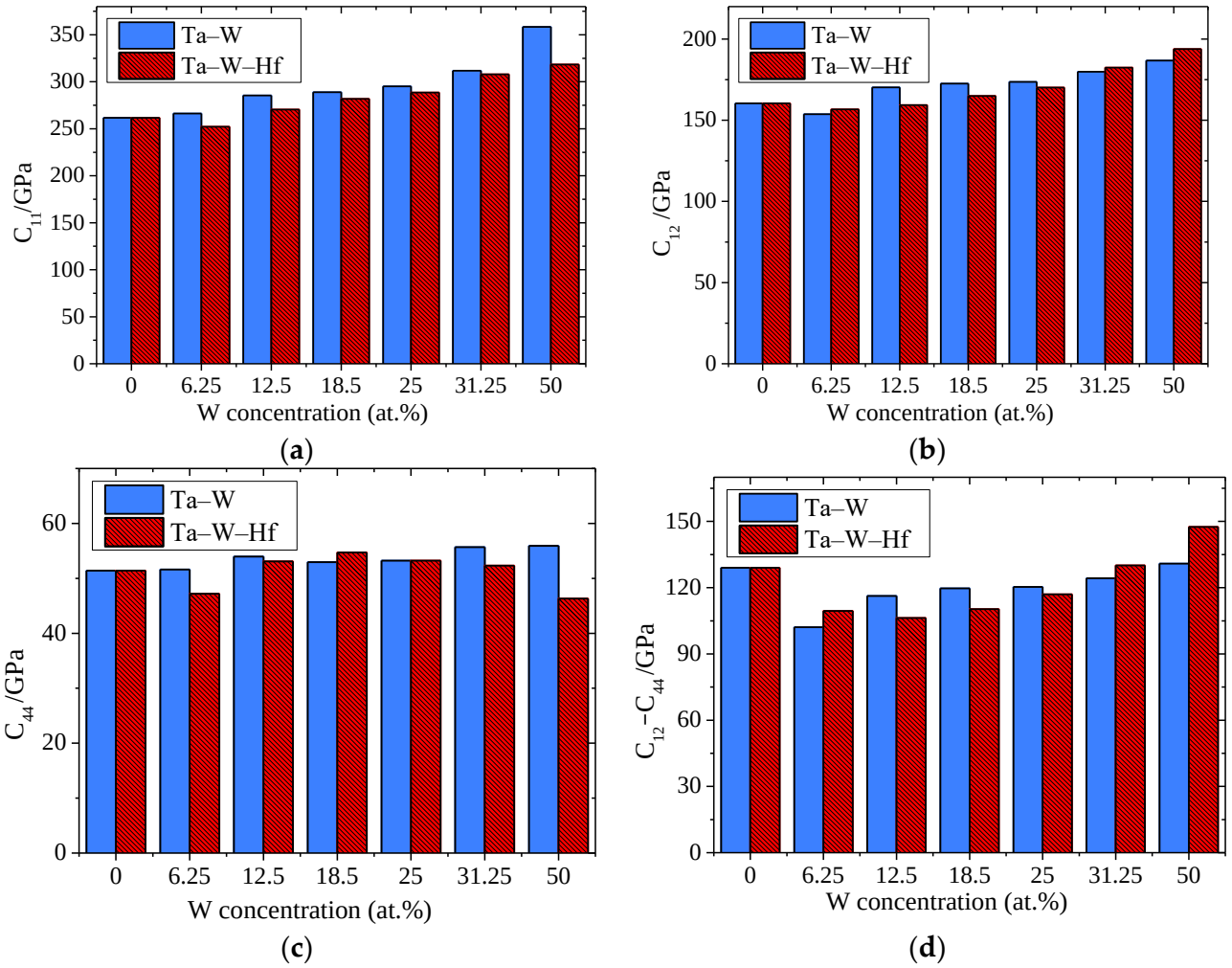

Figure 5. The mechanical constant of Ta–W alloys and Ta–W–Hf alloys with different W content. (**a**) C_{11}, (**b**) C_{12}, (**c**) C_{44}, (**d**) C_{12}–C_{44}.

Table 4. The calculated elastic constants of Ta–W alloys and Ta–W–Hf alloys with different W content (unit: GPa).

Alloy	B	G	E	B/G	σ	A	Note
Ta	194.16	51.11	140.95	3.80	0.35	1.01	Present
Ta	193.60	54.9	150.4	3.53	0.34	1.10	Cal [31]
Ta	204.20	59.82	163.50	3.42	0.34	1.14	Cal [23]
Ta	188.26	56.21	155.37	3.35	0.33	1.58	Exp [32]
Ta–6.25W	191.24	53.42	146.60	3.58	0.34	0.92	Present
Ta–12.50W	208.66	55.40	152.70	3.77	0.35	0.94	Present
Ta–18.75W	211.41	55.00	151.82	3.84	0.35	0.91	Present
Ta–25.00W	214.10	56.11	154.82	3.82	0.35	0.88	Present
Ta–25.00W	226.94	63.92	175.29	3.55	0.34	0.85	Cal [23]
Ta–31.25W	223.90	59.58	164.18	3.76	0.35	0.84	Present
Ta–50.00W	243.98	66.42	182.67	3.67	0.35	0.65	Present
Ta–50.00W	243.98	80.96	219.71	3.16	0.33	0.84	Cal [23]
Ta–6.25W–6.25Hf	188.47	47.41	131.22	3.98	0.36	0.99	Present
Ta–12.5W–6.25Hf	196.35	54.05	148.52	3.63	0.34	0.96	Present
Ta–18.75W–6.25Hf	203.92	56.17	154.35	3.63	0.34	0.94	Present
Ta–25.00W–6.25Hf	209.62	55.52	153.06	3.78	0.35	0.90	Present
Ta–31.25W–6.25Hf	224.23	56.26	155.75	3.99	0.36	0.83	Present
Ta–50.00W–6.25Hf	235.37	52.17	145.73	4.51	0.37	0.74	Present

The shear modulus and Young's modulus of the Ta–W–Hf alloy show a trend of increasing and then decreasing with the increase in W content. When W concentration is less than 31.25%, the shear modulus and Young's modulus of the Ta–W–Hf alloy increase with the increasing W content. When the W content reaches 31.25%, the shear modulus and Young's modulus of the Ta–W–Hf alloy increase by 51.9% (G) and 42% (E), respectively, compared to pure Ta. When the W content over 31.25%, the shear modulus of Ta–W–Hf decreases from 56.26 GPa of Ta–31.25W–6.25Hf to 52.17 GPa of Ta–50W–6.25Hf, a decrease of 7.3%. The trend of Young's modulus is similar to that of shear modulus: the Young's modulus decreases from 155.75 GPa (W = 31.25%) to 145.73 GPa (W = 50%) with a decrease of 6.4%. The rate of decrease in Young's modulus is lower than that of shear modulus, however the shear modulus and Young's modulus of the Ta–W–Hf alloy are still higher than that of the pure Ta.

The shear modulus and Young's modulus correspond to the resistance of the system to shear deformation and the stress required to produce elastic deformation, respectively. The larger the value, the less deformation that occurs. Combined with the data in Figure 6, it can be preliminarily concluded that the strength of the Ta alloy can be improved by doping it with W, and with the increase in W content, the ability of Ta–W alloys to resist external uniform pressure increases, while the strength of the alloy decreases when Hf is added to the Ta–W alloy.

The intrinsic toughness and brittleness of the alloy can be described by physical quantities such as the Poisson's ratio of the material. For Ta alloys, the critical value of Poisson's ratio is 0.26, and Ta alloys exhibit relative toughness when Poisson's ratio is greater than 0.26. Based on the empirical criterion of Pugh [33], the ratio of bulk modulus B to shear modulus G can also be used to measure the tough–brittle behavior of the material, and when $B/G > 1.75$, the material is ductile and vice versa.

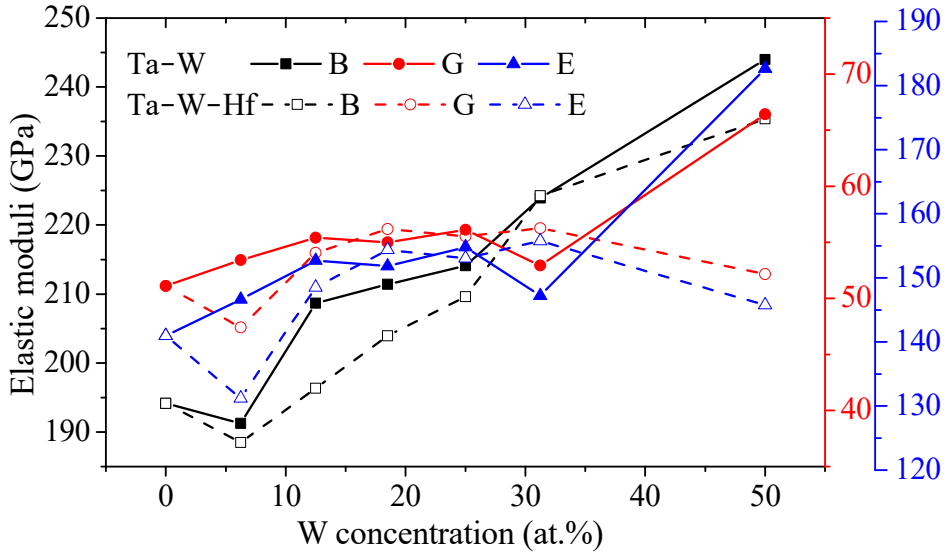

Figure 6. The calculated elastic constant of Ta–W alloys and Ta–W–Hf alloys with different W content (unit: GPa).

Figure 7 shows the B/G and Poisson's ratio value of Ta–W and Ta–W–Hf alloys with different W contents. It can be seen that the B/G and Poisson's ratio changes remain consistent, and the ratios are greater than the critical value, which indicates that the Ta–W–Hf alloy is ductile. In the Ta–W alloy, the B/G and Poisson's ratio increases with the increase in W content, and the changes in B/G and Poisson's ratio curves are not significant when the W content is greater than 18.75%. When Hf is added to the Ta–W alloy, the B/G and Poisson's ratios vary widely; the B/G and Poisson's ratios decrease and then increase with the increasing W content. When the W content is between 12.25% to 25%, the B/G and Poisson's ratios of Ta–W–Hf alloys with the same W content are lower than those of Ta–W alloys. When the W content is greater than 25%, the B/G and Poisson's ratios increase sharply with the increase in W content, which shows that the addition of Hf to the Ta–W alloy can significantly improve the toughness of the alloy.

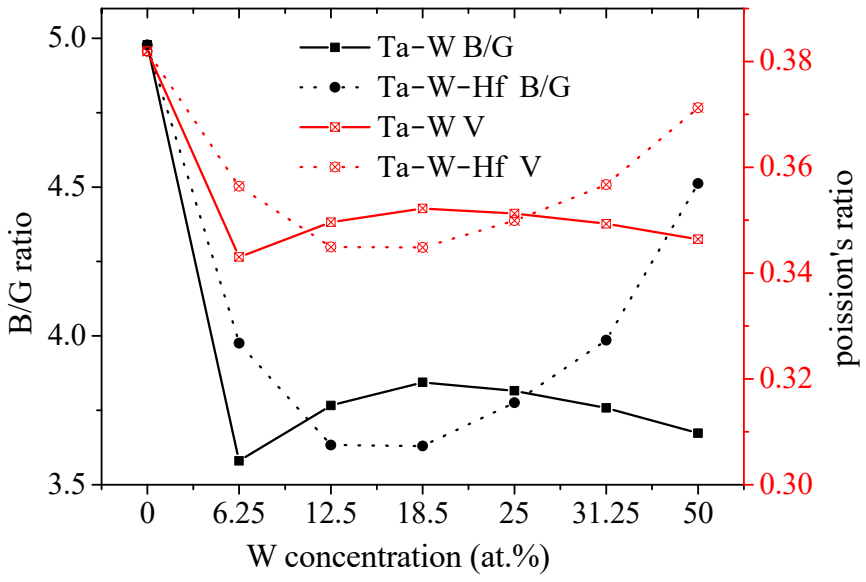

Figure 7. The B/G and Poisson's ratio value of Ta–W and Ta–W–Hf alloys with different W contents.

3.3.2. Elastic Anisotropy

Elastic anisotropy is closely related to the microcracks of materials. The elastic anisotropy index can quantitatively determine the anisotropy of materials, thus, studying the mechanical properties of materials in different directions has important application value in materials research. A^u, A_B, and A_G are general elastic anisotropy factors and the percentage of anisotropy in compression and shear, respectively, which reflect the degree of anisotropy of chemical bonding between atoms in different planes of the crystal structure. These are defined as:

$$A^u = 5\frac{G_v}{G_R} + \frac{B_V}{B_R} - 6 \tag{11}$$

$$A_B = \frac{B_V - B_R}{B_V + B_R} \tag{12}$$

$$A_G = \frac{G_v - G_R}{G_v + G_R} \tag{13}$$

For isotropic material, the zero value of A^u, A_B, and A_G represent the material as isotropic. The larger the difference from zero, the greater the degree of anisotropy of the material. The calculated anisotropy factor of the Ta–W–Hf alloy phase is shown in Table 5. When W is added to Ta, both indices (A^u and A_G) increase with increasing W content, while the increase in anisotropy factor is smaller when Hf is added to the Ta–W alloy, which indicates that the doping of Hf elements in Ta–W–Hf alloys can reduce the anisotropy of the material.

Table 5. Calculation results of the anisotropic factors A^u , A_B, A_G of Ta–W–Hf alloys.

Alloy	A^u	A_B	A_G
Ta	0.0264	0	0.0026
Ta–6.25W	0.0090	0	0.0009
Ta–12.50W	0.0052	0	0.0005
Ta–18.75W	0.0107	0	0.0011
Ta–25.00W	0.0211	0	0.0021
Ta–31.25W	0.0346	0	0.0035
Ta–50.00W	0.2228	0	0.0218
Ta–6.25W–6.25Hf	0.0002	0	0.0000
Ta–12.5W–6.25Hf	0.0024	0	0.0002
Ta–18.75W–6.25Hf	0.0053	0	0.0005
Ta–25.00W–6.25Hf	0.0136	0	0.0014
Ta–31.25W–6.25Hf	0.0397	0	0.0040
Ta–50.00W–6.25Hf	0.1061	0	0.0105

The anisotropy can be expressed by plotting the three-dimensional Young's modulus surface in the crystal direction. For isotropic materials, the three-dimensional surface plot is circular–spherical, and the larger the anisotropy, the more the surface plot deviates from spherical. The three-dimensional anisotropy diagrams of Young's modulus of Ta–W and Ta–W–Hf alloys are shown in Figures 8 and 9, respectively. On the diagrams, [100], [010], and [001] represent the X, Y, and Z axes, respectively. The Young's modulus is smaller the closer it is to the origin of the spatial coordinate system. It can be seen that the anisotropy diagrams gradually deviate from the spherical shape with the increasing concentration of W. When the W content is at 50%, the anisotropy diagrams significantly deviate from the spherical shape, which indicates that the Young's modulus shows clear anisotropy with the increasing concentration of W. The anisotropy tends to be more spherical when Hf is added to the Ta–W alloy, indicating that the Ta–W alloy with Hf can reduce the anisotropy of the material. The anisotropy of the Ta–W–Hf alloy is smaller than that of Ta–W with the same W content. The three-dimensional Young's modulus plot is consistent with the anisotropy parameters calculated in Table 5.

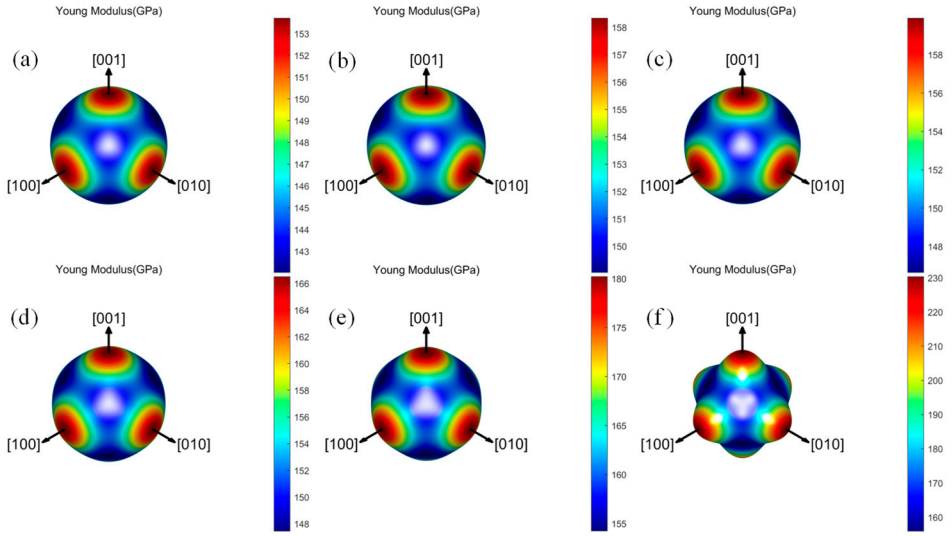

Figure 8. The Young's modulus 3D surface of Ta–W alloys with different W contents: (**a**) Ta–6.25W, (**b**) Ta–12.5W, (**c**) Ta–18.75W, (**d**) Ta–25.00W, (**e**) Ta–31.25W, (**f**) Ta–50.00W.

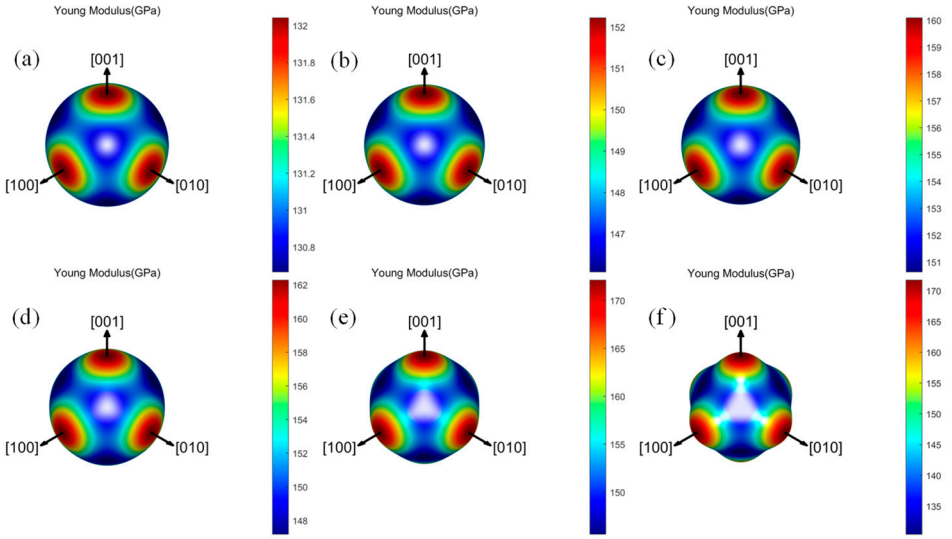

Figure 9. The Young's modulus 3D surface of Ta–W–Hf alloys with different W contents: (**a**) Ta–6.25W–6.25Hf, (**b**) Ta–12.5W–6.25Hf, (**c**) Ta–18.75W–6.25Hf, (**d**) Ta–25.00W–6.25Hf, (**e**) Ta–31.25W–6.25Hf, (**f**) Ta–50.00W–6.25Hf.

3.4. Electronic Properties

In order to further understand the bonding relationship between elements in Ta–W alloys and Ta–W–Hf alloys, the total density of states of Ta–W alloys and Ta–W–Hf alloys with different doping contents were calculated. As shown in Figures 10 and 11, the dotted line represents the position of the Fermi level, and it can be seen that the trend of the total density of states distribution of Ta–W alloys and Ta–W–Hf alloys with different doping contents is basically the same, and the value of the electronic density of states at the Fermi energy level are not zero, which indicates that Ta–W–Hf alloys are as metallic and conductive as Ta–W alloys. At the same time, there are obvious spikes on both sides of the Fermi energy level, indicating the existence of the pseudo-energy gap. The pseudo-energy gap can directly reflect the strength of bonding covalency of the system, and the wider the pseudo-energy gap, the stronger the covalency. From Figure 11, it can be seen that the width of the pseudo-energy gap increases with the increase in W content in the Ta–W–Hf alloy, indicating that the covalency of the Ta–W–Hf alloy gradually becomes stronger with the increase in W content. The TDOS near the Fermi level of the Ta–W–Hf alloy is mainly

derived from the contribution of Ta-d and W-d orbital electrons, and the bonding valence electrons are mainly distributed in the energy range from −5 eV to 5 eV, in which there are strong resonances between the electron orbitals. It is shown that the phase stability and mechanical properties of Ta–W–Hf alloys are closely related to the d orbital electrons.

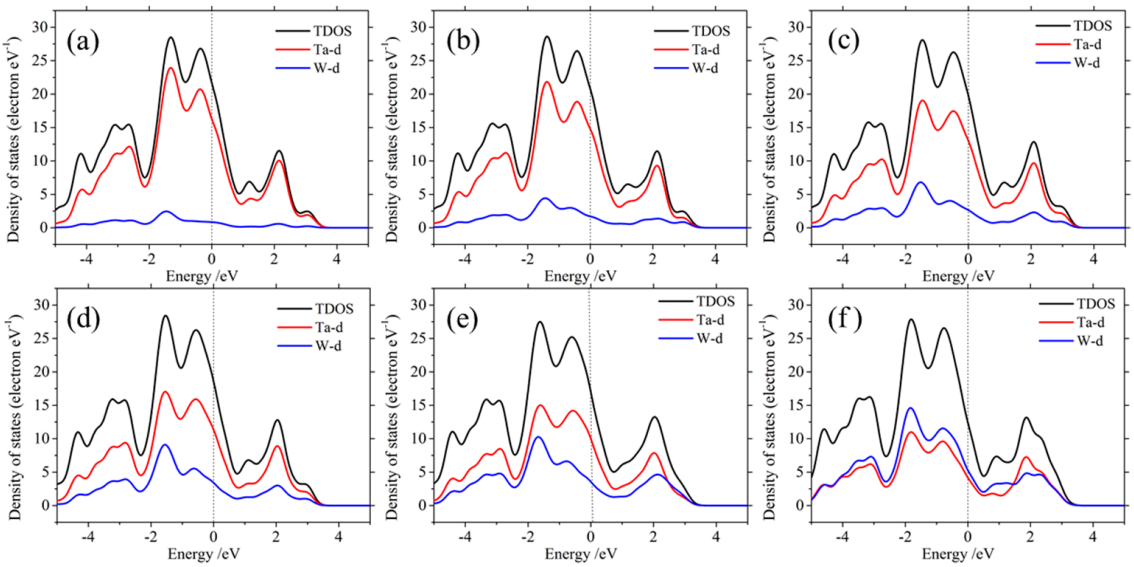

Figure 10. The partial density of states (PDOS) of Ta and W atoms in Ta–W alloys: (**a**) Ta–6.25W, (**b**) Ta–12.5W, (**c**) Ta–18.75W, (**d**) Ta–25.00W, (**e**) Ta–31.25W, (**f**) Ta–50.00W.

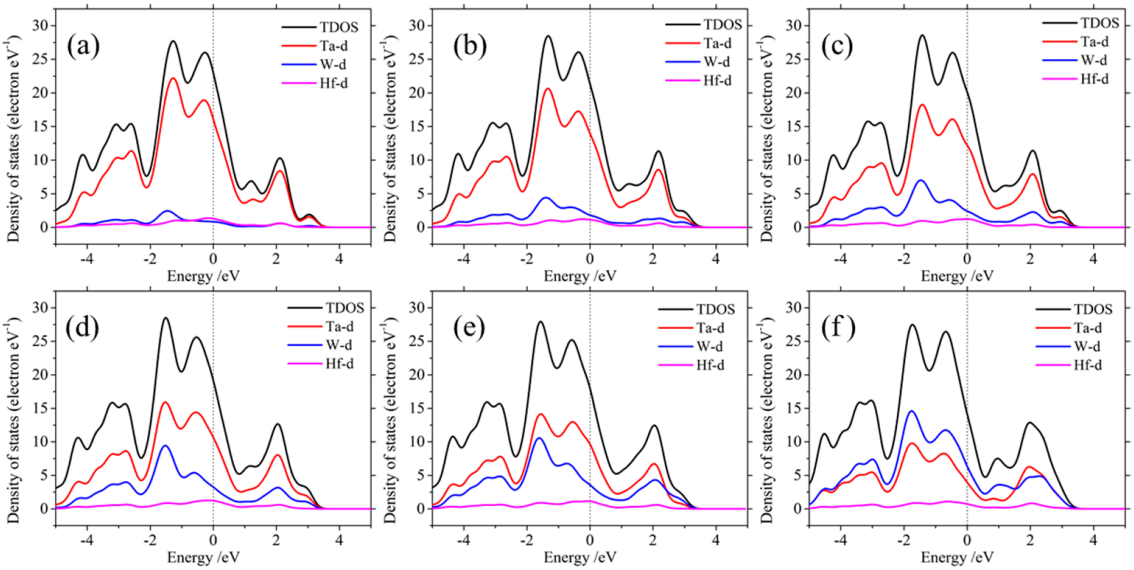

Figure 11. The partial density of states (PDOS) of Ta, W, and Hf atoms in Ta–W–Hf alloys: (**a**) Ta–6.25W–6.25Hf, (**b**) Ta–12.5W–6.25Hf, (**c**) Ta–18.75W–6.25Hf, (**d**) Ta–25.00W–6.25Hf, (**e**) Ta–31.25W–6.25Hf, (**f**) Ta–50.00W–6.25Hf.

The lower the DOS value at the Fermi energy level, the more stable the system is. The DOS values of Ta–6.25W, Ta–12.50W, Ta–18.75W, Ta–25.00W, Ta–31.25W, and Ta–50.00W alloys at the Fermi energy level are 21.70, 20.81, 19.82, 18.76, 17.16, and 12.32, respectively. The DOS values of Ta–6.25W–6.25Hf, Ta–12.50W–6.25Hf, Ta–18.75W–6.25Hf, Ta–25.00W–6.25Hf, Ta–31.25W–6.25Hf, and Ta–50.00W–6.25Hf alloys at the Fermi energy level are 22.90, 21.27, 20.10, 19.12, 17.86, and 14.26, respectively. The stability of the Ta–W alloy gradually increases with the increase in W content; while when Hf is added to the Ta–W alloy, the

DOS value corresponding to the position of the Fermi level of Ta–W–Hf alloys with the same W content increases, indicating that the addition of Hf can reduce the stability of Ta–W alloys with the same Ta–W alloy content, which is consistent with the variation pattern of formation energy and binding energy.

4. Conclusions

In this work, the structural stability, electronic structure, and elastic anisotropy of Ta–W–Hf alloys have been studied by first principles, and the following conclusions were drawn:

(1) All the model are established using the supercell method. It is shown that the stability of the Ta–W–Hf alloy increases with the increase in W content, while the structural stability of the alloys decreases when Hf elements are added to Ta–W alloys;
(2) Both the Ta–W and Ta–W–Hf alloys calculated in this work maintain mechanical stability. For the elastic constants, bulk modulus, shear modulus, Young's modulus, and anisotropy of the materials, the Ta–W alloy shows a tendency to increase consistently with increasing W content, while the Ta–W–Hf alloy shows a tendency to increase and then decrease. For Young's modulus and shear modulus of the materials, the highest values are found for Ta–31.25W–6.25Hf;
(3) When the W content is over 25%, the B/G and Poisson's ratio of the Ta–W–Hf alloy are higher than those of the Ta–W alloy with the same W content, and the addition of Hf increases the ductility of the alloy.

Author Contributions: X.R. and S.Z.: conceptualization, methodology, software, validation, writing—original draft preparation and editing; S.H. and Q.C.: supervision and project administration; W.L. and Y.W.: formal analysis and data curation. All authors have read and agreed to the published version of the manuscript.

Funding: This work was funded by Southwest Technology and Engineering Research Institute (QH202208).

Data Availability Statement: All data in this work are stored at Southwest Technology and Engineering Research Institute.

Conflicts of Interest: The authors declare no conflict of interest.

References

1. Rieth, M.; Dudarev, S.L.; de Vicente, S.M.G.; Aktaa, J.; Ahlgren, T.; Autusch, S.; Armstrong, D.E.J.; Balden, M.; Baluc, N.; Barthe, M.F.; et al. Recent progress in research on tungsten materials for nuclear fusion applications in Europe. *J. Nucl. Mater.* **2013**, *432*, 482–500. [CrossRef]
2. Knaster, J.; Moeslang, A.; Muroga, T. Materials research for fusion. *Nat. Phys.* **2016**, *12*, 424–434. [CrossRef]
3. Kaufmann, D.; Monig, R.; Volkert, C.A.; Kraft, O. Size dependent mechanical behaviour of tantalum. *Int. J. Plast.* **2011**, *27*, 470–478. [CrossRef]
4. Novakowski, T.J.; Tripathi, J.K.; Hassanein, A. Effect of high-flux, low-energy He+ ion irradiation on Ta as a plasma-facing material. *Sci. Rep.* **2016**, *6*, 1–10. [CrossRef]
5. Brooks, J.N.; El-Guebaly, L.; Hassanein, A.; Sizyuk, T. Plasma-facing material alternatives to tungsten. *Nucl. Fusion* **2015**, *55*, 043002. [CrossRef]
6. Browning, P.N.; Alagic, S.; Carroll, B.; Kulkarni, A.; Matson, L.; Singh, J. Room and ultrahigh temperature mechanical properties of field assisted sintered tantalum alloys. *Mater. Sci. Eng. A-Struct. Mater. Prop. Microstruct. Process.* **2017**, *680*, 141–151. [CrossRef]
7. Li, X.B.; Xie, Y.Q. Valence bond structure of Ta-W alloys. *Acta Metall. Sin.-Engl. Lett.* **2009**, *22*, 275–283. [CrossRef]
8. Lv, Y.N.; Hu, K.G.; Huang, Z.; Cao, Z.L.; Wen, S.L.; Zhao, Y.; Pan, M.; Deng, H.Q. Effect of tungsten on the vacancy behaviors in Ta-W alloys from first-principles calculations. *Solid State Commun.* **2020**, *306*, 113767. [CrossRef]
9. Wang, S.; Wu, Z.H.; Xie, M.Y.; Si, D.H.; Li, L.Y.; Chen, C.; Zhang, Z.; Wu, Y.C. The effect of tungsten content on the rolling texture and microstructure of Ta-W alloys. *Mater. Charact.* **2020**, *159*, 110067. [CrossRef]
10. Zhang, X.; Tian, J.; Xue, M.T.; Jiang, F.; Li, S.Z.; Zhang, B.Z.; Ding, J.; Li, X.P.; Ma, E.; Ding, X.D.; et al. Ta W Refractory Alloys with High Strength at 2000 degrees C. *Acta Metall. Sin.* **2022**, *58*, 1253–1260. [CrossRef]
11. Ma, G.Q.; Zhao, M.; Xiang, S.; Zhu, W.Q.; Wu, G.L.; Mao, X.P. Effect of the Severe Plastic Deformation on the Corrosion Resistance of a Tantalum-Tungsten Alloy. *Materials* **2022**, *15*, 7806. [CrossRef] [PubMed]

12. Zielinski, R.E. Electropolrshing of T111 foils for transmission electron-microscopy. *J. Less-Common Met.* **1975**, *40*, 341–343. [CrossRef]
13. Stecura, S. Dissolution kinetics of small amounts of oxygen in tantalum alloy T-111 and internal oxide displacement reactions during annealing. *Oxid. Met.* **1976**, *10*, 291–309. [CrossRef]
14. Zhang, X.M.; Hu, Z.W.; Liu, J.Y.; Bai, X.F.; Tan, S.B.; Li, Z.K.; Zhang, T.J.; Wang, X.C. Strengthening and grain boundary hardening for Ta–W–Hf alloy. *Rare Met. Mater. Eng.* **2007**, *36*, 2156–2159.
15. Zhang, X.M.; Hu, Z.W.; Tian, F.; Yin, T. Tensile Plastic Deformation of Cell Structure Strengthening Ta–9.2W–0.5Hf Alloy. *Rare Met. Mater. Eng.* **2008**, *37*, 1781–1784.
16. Leonard, K.J.; Busby, J.T.; Zinkle, S.J. Microstructural and mechanical property changes in the Ta-base T-111 alloy following thermal aging. *J. Nucl. Mater.* **2007**, *366*, 353–368. [CrossRef]
17. DiStefano, J.R.; McCoy, H.E. Mechanical properties of T-111 at low to intermediate temperatures. *Int. J. Refract. Met. Hard Mater.* **2002**, *20*, 381–387. [CrossRef]
18. Senkov, O.N.; Daboiku, T.I.; Butler, T.M.; Titus, M.S.; Philips, N.R.; Payton, E.J. High-temperature mechanical properties and oxidation behavior of Hf–27Ta and Hf–21Ta–21X (X is Nb, Mo or W) alloys. *Int. J. Refract. Met. Hard Mater.* **2021**, *96*, 105467. [CrossRef]
19. Senkov, O.N.; Daboiku, T.; Butler, T.M.; Rao, S.I.; Payton, E.J. Microstructure, compression properties, and oxidation behavior of Hf–25Ta–5Me alloys (Me is Mo, Nb, W, 0.5Mo+0.5 W, Cr, or Zr). *Int. J. Refract. Met. Hard Mater.* **2022**, *109*, 105968. [CrossRef]
20. Barklay, C.D.; Howe, J.Y.; Kramer, D.P. Investigation of stress rupture tested neutron irradiated tantalum alloys. In *Space Technology and Applications International Forum (STAIF-2008)*; Univ New Mexico, Inst Space & Nucl Power Studies: Albuquerque, NM, USA, 2008; Volume 969, pp. 439–445.
21. Barklay, C.D.; Kramer, D.P.; Talnagi, J. Investigation of effects of neutron irradiation on tantalum alloys for radioisotope power system applications. In *Space Technology and Applications International Forum (STAIF-2007)*; Univ New Mexico, Inst Space & Nucl Power Studies: Albuquerque, NM, USA, 2007; Volume 880, pp. 224–228.
22. Segall, M.D.; Lindan, P.J.D.; Probert, M.J.; Pickard, C.J.; Hasnip, P.J.; Clark, S.J.; Payne, M.C. First-principles simulation: Ideas, illustrations and the CASTEP code. *J. Phys. Condens. Matter* **2002**, *14*, 2717–2744. [CrossRef]
23. Jiang, D.; Wang, Q.; Hu, W.; Wei, Z.; Tong, J.; Wan, H. The effect of tantalum (Ta) doping on mechanical properties of tungsten (W): A first-principles study. *J. Mater. Res.* **2016**, *31*, 3401–3408. [CrossRef]
24. Featherston, F.H.; Neighbours, J.R. Elastic Constants of Tantalum, Tungsten, and Molybdenum. *Phys. Rev.* **1963**, *130*, 1324–1333. [CrossRef]
25. Pan, R.K.; Ma, L.; Bian, N.; Wang, M.H.; Li, P.B.; Tang, B.Y.; Peng, L.M.; Ding, W.J. First-principles study on the elastic properties of B′ and Q phase in Al–Mg–Si (–Cu) alloys. *Phys. Scr.* **2013**, *87*, 015601. [CrossRef]
26. Wu, Y.N.; Li, L.; Cheng, H.P. First Principles Study on Ta25 Low and High-Temperature Phases. In Proceedings of the APS March Meeting 2010, Portland, OR, USA, 15–19 March 2010.
27. Voigt, W.B. Lehrbuch der Kristallphysik. *Teubner Leipz.* **1928**.
28. Watt, J.P.; Davies, G.F.; O'Connell, R.J. The elastic properties of composite materials. *Rev. Geophys.* **1976**, *14*, 541–563. [CrossRef]
29. Born, M.; Huang, K.; Lax, M. Dynamical Theory of Crystal Lattices. *Am. J. Phys. USA* **1985**, *23*, 474. [CrossRef]
30. Xu, W.; Wang, Y.; Wang, C.; Liu, X.; Liu, Z.K. Alloying effects of Ta on the mechanical properties of gamma' Co-3(Al, W): A first-principles study. *Scr. Mater.* **2015**, *100*, 5–8. [CrossRef]
31. Zhang, X.; Li, H.; Xu, Y.; Liu, Q.; Liu, Y. First-principles study on the mechanical properties and thermodynamic properties of Mo–Ta alloys. *Plasma Sci. Technol.* **2020**, *22*, 203–210. [CrossRef]
32. Strachan, A.; Cagin, T.; Gulseren, O.; Mukherjee, S.; Cohen, R.E.; Goddard, W.A. First principles force field for metallic tantalum. *Model. Simul. Mater. Sci. Eng.* **2004**, *12*, S445–S459. [CrossRef]
33. Pugh, S.F. The London, Edinburgh, and Dublin philosophical magazine and journal of science: Series 7. *Phil. Mag.* **1954**, *45*, 823–827. [CrossRef]